Fuel 275 (2020) 117918

Contents lists available at ScienceDirect

Fuel

journal homepage: www.elsevier.com/locate/fuel

Full Length Article

Effect of 5-membered bicyclic hydrocarbon additives on nanostructural disorder and oxidative reactivity of diffusion flame-generated diesel soot

Moataz K. Abdrabou[a,1], Pranay P. Morajkar[a,b,1], Gerardo D.J. Guerrero Peña[c], Abhijeet Raj[a,*], Mirella Elkadi[d], Akshay V. Salkar[b]

[a] Department of Chemical Engineering and Centre for Catalysis and Separation, Khalifa University of Science & Technology, Abu Dhabi, United Arab Emirates
[b] School of Chemical Sciences, Goa University, Taleigao Plateau, Goa, India
[c] Clean Combustion Research Centre, King Abdullah University of Science and Technology, Thuwal, Saudi Arabia
[d] Department of Chemistry, Khalifa University of Science & Technology, Abu Dhabi, United Arab Emirates

ARTICLE INFO

Keywords:
Diesel
5-membered bicyclic additive
Norbornane
Soot
Nanostructure
Oxidative reactivity

ABSTRACT

Soot emission from diesel engines is of serious concern, as it is carcinogenic and remains suspended in air for a long time to cause adverse effects on human health and the environment. A way to reduce soot emission is by altering soot nanostructures by introducing fringe curvatures to enhance reactivity and increase oxidation. Such disorder in soot nanostructure can be initiated by the introduction of 5-membered rings into 6-membered, graphite-like soot structures. This study investigates the effect of the addition of norbornane, a saturated, 5-membered bicyclic hydrocarbon additive to diesel on the physicochemical properties, sooting propensity, structural disorders, and the oxidative reactivity of soot. The physicochemical analysis revealed that the threshold sooting index (TSI) of the blend is reduced to 29.5 at an optimum blending percentage of 10% norbornane-90% Diesel (NBD) as compared to the TSI of 37 for diesel. The analyses using XRD, Raman, HRTEM, and EDX indicated that the addition of this additive resulted in an increased soot nanostructural disorder, smaller PAH size, increased fringe curvature, and significantly greater aliphatic content in soot as compared to an unsaturated 5-membered bicyclic additive, dicyclopentadiene (DCPD). The reactivity studies confirmed that NBD soot is easily oxidized in air, since it requires a lower initial activation energy (90 kJ/mol) as compared to DCPD (120 kJ/mol) and pure diesel soots (170 kJ/mol). Thus, norbornane, a saturated 5-membered bicyclic compound, which is available as a by-product of polymer industry and in crude oil, can serve as a potential fuel additive for designing advanced fuels.

1. Introduction

Fossil fuels are the leading energy source worldwide and will remain the dominant one for several upcoming years. With the continuous increase in the consumption of fossil fuels, more and more pollutants are being generated and released into air. A solid-phase pollutant that is being released in huge amounts on a daily basis is the particulate matter (soot). The term soot, refers to fine, black, carbon-containing particles that are formed due to the incomplete combustion of an organic material. Soot is produced in the form of agglomerates that are generated as a result of coagulation of small spherules/particles, and its size varies from few nanometers to few micrometers [1]. Soot is generated as a result of the partial oxidation of diesel and gasoline fuels inside internal combustion engines. This phenomena occurs as a result of the short timespan available for the fuel to completely oxidize, in addition to the absence of homogeneity in the fuel–air mixture and the variation in temperature inside the engine. Soot is recognized as a mixture of carcinogenic compounds by the International Agency for Research on Cancer, and is one of the leading causes of death [2]. Soot also has detrimental effects on the environment and is considered one of the main contributors to air pollution, regional climate change, and global warming.

The diesel particulate filters (DPFs) in vehicle exhaust system appear as a good technology to detoxify diesel exhaust, as they trap the harmful particulate matter to prevent their emission [3]. The DPFs require frequent regeneration to avoid pressure build up in the exhaust system. According to a study conducted by Brijesh et al. [4], the delay in DPF regeneration led to a large increase in backpressure, and hence,

* Corresponding author.
E-mail address: abhijeet.raj@ku.ac.ae (A. Raj).
[1] Equal contribution by the first two authors.

https://doi.org/10.1016/j.fuel.2020.117918
Received 29 January 2020; Received in revised form 17 April 2020; Accepted 21 April 2020

resulted in a reduction in engine efficiency and an increased emission levels. Since active regeneration process requires an extra amount of fuel injection to increase exhaust gas temperature to burn soot collected in DPF [5], this renders the solution cost ineffective, especially for developing countries. Therefore, the oxidative reactivity of soot must be enhanced by: (a) increasing the oxygen and aliphatic content within soot structure, and (b) producing small PAH layers with high disorder in the graphitic structure and high tortuosity. Most studies in the literature that attempted to reduce the negative impacts of fuels or enhance the soot oxidative reactivity utilized either oxygenated or metal-based additives. However, the proposed solutions either involve high costs due to the use of rare metals as catalysts, or the risk of generating new pollutants such as aldehydes and dioxins (which are highly toxic pollutants). Oxygenated fuels lead to the reduction in the energy density of the blended fuels, and are known to be responsible for corrosion in fuel pumps and filters. For instance, Dias et al. [6] studied the effect of ethanol–benzene blends on soot production. Although, they found that the partial replacement of fuel by ethanol reduced soot precursor concentrations, it also increased the harmful oxygenated emissions such as formaldehyde and acetaldehyde, which are among the well-known volatile organic pollutants in the atmosphere [7–9]. Most of the fuel alternatives such as oxygenated fuels or bio-fuels usually exhibit low cetane number (which is an indicator of the quality of diesel and its ignition properties) [10]. Moreover, oxygenated fuels tend to have less volatility and high lubricity than diesel [11], although light molecules such alcohols or ethers, when added to diesel, lead to increased volatility and reduced lubricity, and often have miscibility problems [12]. Thus, there is a need to find low cost novel additives for fuels with the capabilities to enhance combustion efficiency and reduce particulate matter emission, with a negligible effect on energy density to diminish the impact of fossil fuel combustion on human health and the environment.

Ideally, for reduced soot emissions from engines, soot produced from a blended fuel must contain some physiochemical properties that enhance its oxidative reactivity. Some of these properties are: a) a high concentration of the oxygenated functional groups [13], b) a high ratio of aliphatic to aromatic content within soot, as aliphatics are more reactive and easily oxidized at lower temperature than aromatics, which makes soot particles more prone to oxidation [14]; c) the existence of small graphene layers (fringes) with high tortuosity and random orientations, which deviates the structure from stability and lowers the activation energies for the oxidation of carbon atoms within the soot nanostructure [15]; d) the increase in soot surface area resulting from the small size of primary particles, which reduces mass transfer limitations in accessing reactive site on soot by O_2 (moreover, small primary particles are inherently composed of small aromatic layers with higher ratio of reactive peripheral carbon atoms to the less-reactive basal carbon atoms as compared to larger aromatic layers [16]), and e) the increase in the active surface area of soot that accounts for the concentration of radicals sites on soot and the structural defects, which possess high binding energy for oxygen and support soot oxidation process through its chemisorption [17].

Recently, some studies in the literature have emphasized on the introduction of 5-membered cyclic structures within the soot's 6-membered aromatic planes to impose curvature in the soot structure, so as to make it more disordered and thus prone to oxidation [18–21]. The formation of five-membered cyclic compounds during combustion depends on the kinetics and thermodynamic factors of high temperature assisted, complex mechanism of PAH formation and growth in flames. A flame study [22] using dicyclopentadiene (DCPD), which is an unsaturated bicyclic additive (see Fig. 1A), showed that Threshold Sooting Index (TSI) of diesel reduces with increase in DCPD concentration up to 10% (v/v). However, the further increase in DCPD concentration results in an increase in the sooting tendency. A similar non-linear trend was shown by the cetane number of the blended fuels. It was also observed that the disorder in the soot structure is enhanced by the addition of DCPD. Thus, it appears that, with the aid of 5-membered cyclic additives, it is possible to increase soot oxidation inside engines, and consequently, (a) reduce emission of soot in the exhaust, and (b) achieve efficient regeneration of particulate filters.

Norbornane, also known as bicyclo [2.2.1] heptane, is a saturated hydrocarbon and contains, two 5-membered bridged cyclic ring structure (see Fig. 1A). It is commercially produced by the reaction of dicylcopentadiene with ethylene via Diels-Alder reaction. Both norbornane and DCPD are found in the distillation cuts of oil refineries. Therefore, it is hypothesized that the addition of such a bicyclic, saturated, 5 membered ring structure to diesel fuel can influence the radical formation kinetics and oxidation chemistry of diesel, and probably enhance the formation and introduction of 5 membered cyclic structure into the 6-membered graphitic planes, thus distorting the soot structure from fringe planarity, leading to increased curvature (tortuosity). More importantly, in comparison to unsaturated 5 membered cyclic additives, the saturated bicyclic additives such as norbornane may result in a greater aliphatic content of soot, thus exhibiting its increased reactivity. Such a comparative analysis is not available in the literature to the best of our knowledge.

The above hypothesis is put to test in the present investigation by performing systematic studies such as the optimization of norbornane blending ratio with diesel (termed as NBD), its influence on physicochemical properties of the fuel blend, the sooting propensity, and its influence on the chemical and morphological characteristics of soot nanostructures and on the oxidative reactivity of soot particles. A comparative analysis of soot nanostructural properties of NBD and DCPD is also presented to determine the effect of saturated and unsaturated 5 membered bicyclic additives on structural disorder, aliphatic/aromatic composition, oxidative reactivity of soot, soot emission tendency of diesel.

2. Experimental methodology

Smoke point measurement is one of the standard lab scale method of analyzing the tendency of the fuel to generate soot, and it is a good indicator for actual diesel engine emissions [23]. Smoke point is defined as the flame height at which the sooting wings start to be visible in the diffusion flame of smoke point apparatus [24]. Also, its inverse, the threshold sooting index (TSI) correlates very well with the actual particulate emissions and gives more representative information [25]. The smoke point apparatus was selected for soot study in this paper, as it produces stable flames with known fuel flow rates that allows the soot particle collection at various flame heights above the smoke point. While the study presented in this paper can also be conducted using a diesel engine, several engine operating parameters such as engine speed, load, fuel injection, and exhaust gas recirculation along with the changes in fuel properties such as density, viscosity, and cetane number upon blending simultaneously influence the soot formation, oxidation, and its nanostructural characteristics [15,26,27,28]. This makes it complicated to derive a confirmative evidence that can specifically highlight the sole effect of the fuel additive and its chemical structure on the sooting tendency of the fuel blend and on soot nanostructures and reactivity. Therefore, smoke point apparatus was preferred considering the objective of this investigation. Smoke point measurements were performed according to the standard ASTM D1322-08 procedure [29]. In this test, soot particles were generated in the diffusion flames of diesel and its blends at atmospheric pressure by means of a smoke point apparatus (RAP172) installed in a fume hood. A detailed representation of the smoke point setup is shown in Fig. 1. The smoke point apparatus consists of: i) a cylindrical fuel reservoir that contains the fuel to be tested, ii) a cotton wick tube, which remains soaked in the fuel reserve and is burned at its tip to generate smoke, iii) a lamp body, which surrounds the flame, and contains a metallic ruler behind the flame and a glass door in front of the flame, and iv) a burner holder with a long chimney. The upper end of the chimney contains a perpendicularly

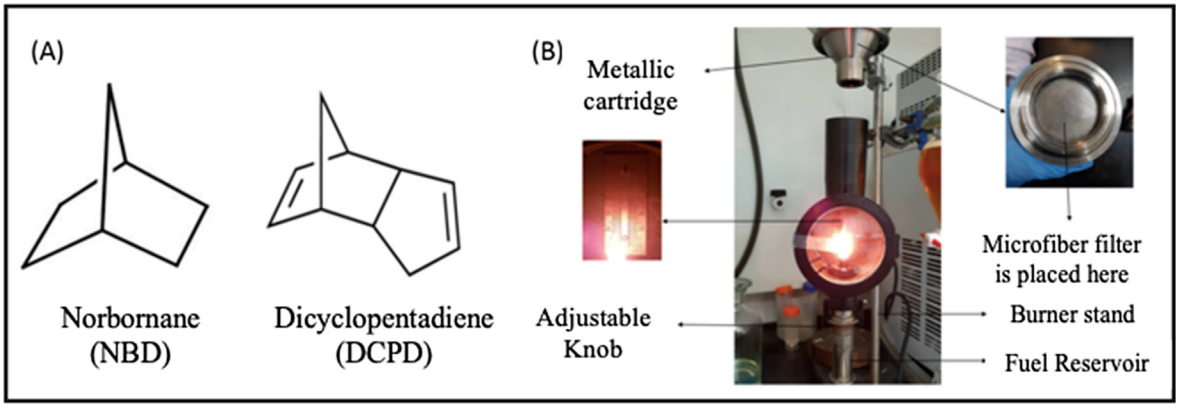

Fig. 1. A) Molecular structure of NBD and DCPD; B) experimental setup for smoke point tests.

mounted-borosilicate microfiber filter enclosed assembly (from Sierra Instruments, USA) that is coupled to a suction pump to allow trapping of soot particles on the filter. This microfiber filter was chosen because of its inertness to PAH, and because of the easiness of handling it to extract soot particles [30]. The lamp body in-houses the burner and minimizes flame disturbances in the fume cupboard and the curved glass window prevents the formation of multiple flame images.

The setup also contains a concentric hole inside the fuel reservoir that provide an opening for the cotton wick height to be adjusted with the aid of the circular knob. The flame extent is measured from the bottom of the exposed wick to the flame tip using the metallic ruler scale behind the flame that ranges from 0 to 50 mm. The flame vertical height can be altered by increasing or decreasing the length of the wick exposure with the aid of the circular knob. This act also leads to either increasing or decreasing the fuel flow rate to the flame accordingly. The adsorbed water and volatiles from the collected soot samples are removed by heating the samples at a rate of 20 °C/min at 400 °C under N_2 flow, and then subjected to morphological and chemical characterization.

The transmission electron microscope (Tecnai T20 electron microprobe) operating at 200 kV accelerating voltage with an ultimate lattice resolution of 0.24 nm was used to record microstructural details of soot particles. After ultra-sonicating in ethanol for 10 min, the soot samples were placed on a lacey carbon-coated, copper grid. The Gatan Image Filter in the STEM mode with the energy resolution of 1 eV was used to record the electron energy loss spectra (EELS), which provided the information about relative distribution of σ and π bonds in the soot structure.

In order to study the oxidative reactivity of soot in air, thermogravimetric analyzer (TGA, NETZSCH STA 409PC-LUXX) was used. The dried soot samples were subjected to temperature programmed heating in air from 200 to 800 °C at different heating rates of 1, 3, and 5 °C/min to oxidize soot in each experiment [30].

The structural parameters of soot were obtained using the X-ray diffraction patterns in the range of 10–90° with a step size of 0.02° using the Panalytical Empyrean X-ray diffractometer (XRD) [30]. The XRD results were used to calculate L_a (the length of the PAHs), L_c (the thickness or the height of the stack), and d_{002} (the spacing between graphene layers). The Raman spectra were recorded using the Witech Alpha 300 RAS equipped with 515 nm laser source and a dual purpose 50x objective lens and the disorder and graphitization in soot samples were analyzed. The Raman spectra was de-convoluted in the Origin Pro software to determine the contribution from different peaks to the overall band, all of which are discussed in detail in the subsequent sections.

3. Results and discussion

3.1. Fuel physical properties

The commercial diesel fuel (Grade No. 2-D S15, ASTM D975 [31]) was obtained from a local fuel station from Abu Dhabi, UAE. Norbornane was procured from Sigma–Aldrich with a purity of ≥ 95%). Norbornane-diesel blends were prepared with 5%, 10%, 15% and 20% norbornane volume fraction in diesel, and were labelled as NBD5, NBD10, NBD15, and NBD20, respectively. All fuel blends were prepared and stored at 25 °C to ensure phase stability over 1 h, before testing on smoke point apparatus. A complete miscibility of the additive in the fuel blend was observed at the above-mentioned compositions without any phase separation. The physical properties of diesel and the NBD blends were measured, as displayed in Table 1. The Stabinger Viscometer (SVM™ 3000, Anton Paar) was used to measure the kinematic viscosity and density of the fuel blends following the procedure as per ASTM D7042 standard [22].

As evident from Table 1, as the concentration of norbornane in the NBD blend increases, the density of the fuel blend increases; while the viscosity and the molecular weight of the fuel blend decreases. This trend is expected as the norbornane additive originally has a higher density and a lower viscosity than pure diesel. Both density and viscosity play a crucial role in engine performance, as they determine the fuel atomization rate during spray injection [32]. Moreover, the improved combustion of the fuel blend also results in suppression of soot production in engines.

3.2. Measurement of smoke point and the threshold sooting index (TSI)

The smoke points of pure diesel and norbornane blends were measured using the ASTM D1322 apparatus and procedure. An increase in the smoke point serves as an indicator that the fuel needs a higher flame height or fuel flow rate to generate soot particles [29]. Thus, a fuel with higher smoke point is considered cleaner with less tendency to produce soot. As observed in Fig. 2, with the addition of small blending percentage of norbornane (up to 10%) to diesel, the smoke point of the NBD blends increases to 22 (± 1) mm from 19 (± 1) mm for pure diesel. The smoke point values undergo a steady decease as the concentration of the additive is further increased. The saturation of fuel

Table 1
Physicochemical properties of diesel and norbornane-diesel blends.

Fuel properties	Diesel	NBD5	NBD10	NBD15	NBD20
Molecular weight (g/mol)	206.00	200.51	195.29	190.34	185.63
Density at 25 °C (g/ml)	0.829	0.831	0.8326	0.834	0.8355
Dynamic viscosity (kg/m.s)	0.00289	0.00276	0.00256	0.00245	0.00235

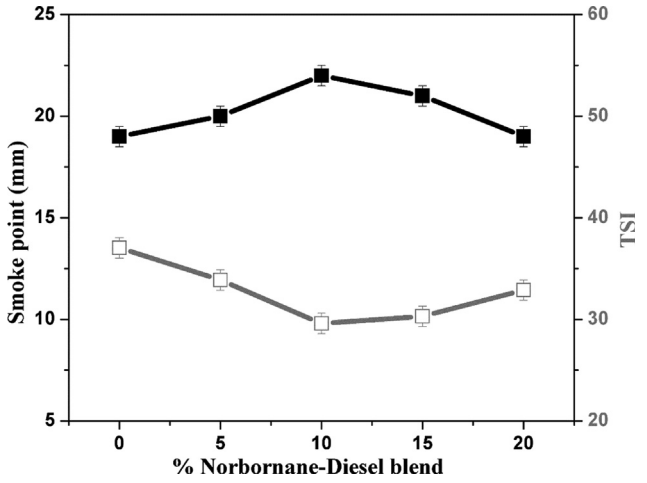

Fig. 2. Variation in smoke point and TSI values of NBD blend.

blend occurs at around 40%, as no further additive can be dissolved in diesel. However, since the smoke point values are apparatus dependent, the threshold sooting index (*TSI*), which is an instrument independent quantity, is calculated for more realistic and practical comparison of the sooting tendencies of fuel blends. The *TSI* was initially introduced by Calcote and Manos [33], who utilized it instead of the smoke point to analyze the experimental results. The authors defined the *TSI* as a sooting index in which "0″ represent the minimum sooting ability and "100" represents the maximum sooting tendency. *TSI* is a linear function of the molecular weight (*MW*) of the fuel and the reciprocal of the smoke point (*SP*), and is represented as: $TSI = a\ (MW/SP) + b$. The two constants, a and b, are apparatus dependent that are found by calibrating the apparatus with known chemical compounds. For our apparatus, their values were calculated as $a = 3.7623$ and $b = -3.7539$ in a previous study [23]. From the TSI curve in Fig. 2, it is evident that the lowest *TSI* values are obtained at an optimum bending percentage of 10%.

Since the average smoke points of pure diesel and 10% NBD blend were in the range of 18–23 mm, the soot from the two fuels was collected at a fixed flame height of 25 mm (i.e., above the smoke points of the two), and were labelled as diesel soot (D) and 10% NBD blend soot (NBD10). The collected soot samples were subjected to detailed characterization tests in order to understand the effect of norbornane additive on the physiochemical structure of soot and its oxidative reactivity.

3.3. Thermogravimetric analysis (TGA)

The soot oxidation tendency in air is a crucial parameter in determining the soot reactivity especially in the DPF. Lower the activation energy, higher is the DPF regeneration efficiency. Therefore, in order to measure the soot's oxidative reactivity, thermogravimetric analyses were performed on the soot samples. The variation in oxidative soot conversion (α) versus temperature as a function of the heating rates for pure diesel soot and NBD10 were measured and plotted in Fig. 3. Soot conversion (α) is defined as $\alpha = \frac{(Mo - M_T)}{(Mo - M_L)}$, with M_O being the initial mass of dry soot, M_T is the mass of partially oxidized soot at oxidation temperature T, and M_L is the leftover mass (mainly ash). M_L in this case was zero, as there was no left-over ash after the complete oxidation of soot. With increasing heating rate, the soot conversion curve shifts towards higher temperature. This phenomenon occurs mainly due to two reasons [34]: (a) There always exists a temperature gradient between the heated air and the carbon sample due to heat transfer limitations and delay. This gradient increases with increasing heating rate, and the resulting heat transfer delay causes the shifting of the thermogravimetric curves towards higher temperature. (b) As the heating rate is

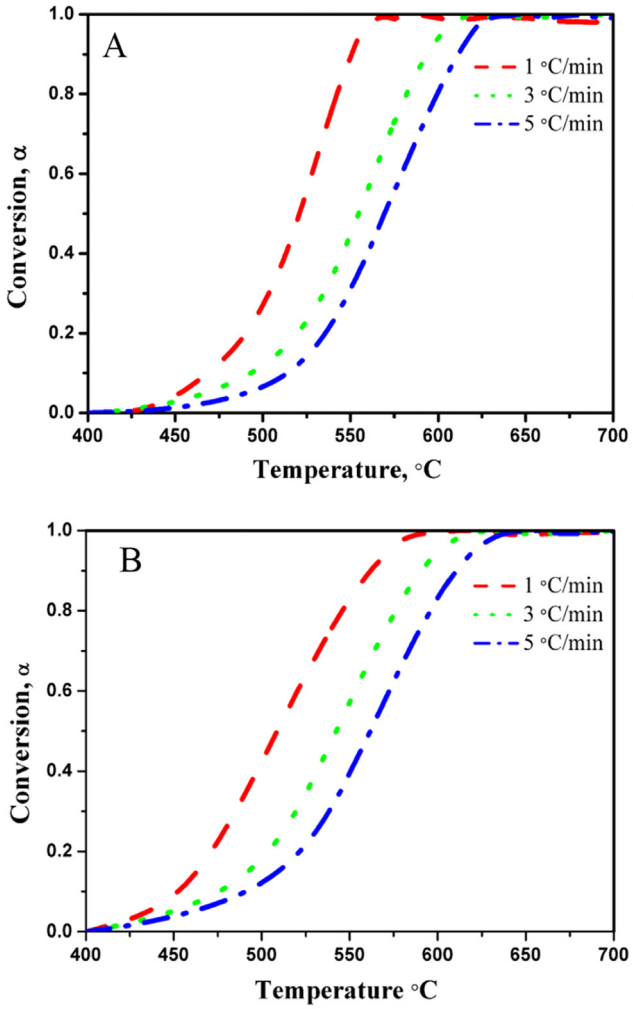

Fig. 3. Soot conversion vs temperature at various heating rates for a) diesel soot b) NBD10 soot.

increased, the time available for a sample to reach a given temperature and react with O_2 at that temperature is shortened. This reaction delay causes the same soot conversion level to be achieved at a higher temperature with a higher heating rate.

To compare the oxidative conversion profiles of diesel and NDB10 soots, the temperatures corresponding to oxidation at an initial stage (i.e. 10% conversion), at 50% conversion, and at 95% conversion stages are given in Table 2. For 10% conversion, NBD10 soot required significantly lower oxidation temperature (around 15–20 °C less) than the diesel soot at heating rates of 1, 3, and 5 °C/min. A similar trend continued as the oxidation of soot progressed to 50% conversion level. Thus, the NBD10 soot had higher reactivity towards oxygen than the diesel soot especially at low conversion levels. With further increase in the soot oxidation from 50 to 95%, the relative difference in required oxidation temperature between NBD10 and diesel soot started to decrease, and as the oxidation reached near completion (at 95% conversion), the oxidation temperatures were almost similar for both the soots.

The further analysis of the thermal stability of soot at different conversion levels were performed by calculating the activation energy of soot oxidation using Friedman method [35], where the rate of soot conversion rate, $\frac{d\alpha}{dt}$is related to soot conversion (α) by the following equation:

$$\frac{d\alpha}{dt} = k(T)f(\alpha) \tag{1}$$

Table 2
Characterization results on diesel and NBD10 soots using different techniques. In the TGA results, T represents temperature, α represents soot conversion, and HR represents heating rate.

Sample properties	Diesel soot	NBD10 soot
TGA results		
T at α = 10% (HR = 1 °C/min)	468 °C	452 °C
T at α = 10% (HR = 3 °C/min)	493 °C	475 °C
T at α = 10% (HR = 5 °C/min)	514 °C	489 °C
T at α = 50% (HR = 1 °C/min)	521 °C	509 °C
T at α = 50% (HR = 3 °C/min)	555 °C	542 °C
T at α = 50% (HR = 5 °C/min)	570 °C	562 °C
T at α = 95% (HR = 1 °C/min)	556 °C	572 °C
T at α = 95% (HR = 3 °C/min)	602 °C	601 °C
T at α = 95% (HR = 5 °C/min)	640 °C	636 °C
HRTEM results		
Mean fringe length	3.57 mm	1.8 nm
Mean fringe tortuosity	1.46	1.54
Primary particle diameter	32 nm	21.7 nm
XRD results		
Interlayer spacing, d_{002}	0.369 nm	0.373 nm
Nano-crystallite height, L_c	1.07 nm	0.96 nm
Nano-crystallite width, L_a	3.01 ± 0.5 nm	2.71 ± 0.5 nm
L_c/d_{002} (no. of layers, N)	2.90	2.58
Raman results		
D1 peak intensity, I_{D1}	4.6	6.4
G peak intensity, I_G	4.1	5
I_{D1}/I_G ratio	1.1	1.3
Lattice width, L_a	3.8 ± 0.5 nm	3.3 ± 0.5 nm

Here, $k(T)$ is the rate constant (s^{-1}) of soot oxidation, obeying Arrhenius equation, $k = Ae^{-(Ea/RT)}$, with A being the pre-exponential factor, Ea being the activation energy of soot oxidation, and T is the temperature [36]. The reaction model or conversion function is denoted by $f(\alpha)$. More details about the procedure for activation energy calculation using the soot conversion profiles at different heating rates can be found in [36,37].

A plot of activation energy at different conversion levels as a function of temperature is presented in Fig. 4 for diesel and NBD10 soots. Significant differences in the initial activation energy at low conversion levels were observed, with lowest activation energy of 90 kJ/mol for NBD10 soot and 180 kJ/mol for diesel soot. As the oxidation progressed to higher conversion levels, the activation energy did not change significantly in the case of diesel soot (± 20 kJ/mol), but, in the case of NBD10 a gradual increase in activation energy was observed reaching a value almost similar to that of diesel soot at near complete conversion. The average activation energies were calculated to be around 170 ± 10 kJ/mol for pure diesel and 110 ± 00 kJ/mol

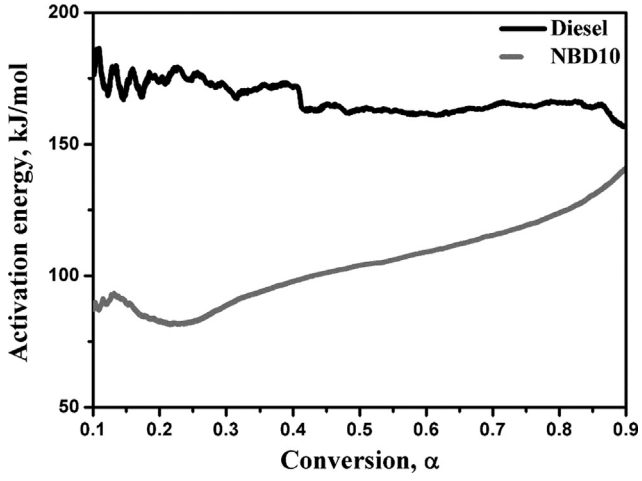

Fig. 4. Variation in activation energy of soot oxidation at different conversion levels for diesel and NBD10 soot.

for NBD soot for the entire oxidation process. The measured activation energies are within the expected range of 100–200 for carbon soots in the literature [38]. The significantly high reactivity of NBD soot at low conversion levels could be due to the presence of higher magnitude of crystal disorder such as shorter fringes with increased fringe tortuosity, leading to a greater percentage of reactive edge carbon atoms as compared to those in diesel soot. Furthermore, the observed increase in activation energy at higher conversion levels in the case of NBD10 soot indicates the presence of higher aliphatic content in NBD soot, which is easily oxidised at temperatures less than 500 °C leaving behind long range PAH molecules in soot, which needs higher temperature and has greater activation energy for reactivity with O_2 [39–41]. Therefore, all the soot samples were subjected to HRTEM, Raman, EDX, XRD, and EELS analyses to obtain more information about C/O content, microstructural disorder, PAH stack size, shape, and σ/ π bonding characteristics of the soot surface, which will be discussed in the subsequent sections.

3.4. High resolution transmission electron microscopy (HRTEM)

Fig. 5 represents the HRTEM images recorded at the resolutions of 20 and 50 nm for diesel (D) and NBD10 soot samples. It is clear from the micrographs that all the soot samples are composed of agglomerated, near spherical particles that are known as primary soot particles. The adjacent particles appear to be fused together due to sintering effect. The primary particle consist of a core–shell like structure, wherein the core is formed due to curved short fringes, whereas long range fringes are concentrically arranged along the periphery to form a shell-like structure [42,43]. The excessive internal oxidation of soot is the reason for the formation of short core fringes with high structural disorder as the soot particles travel through the flame length, which is in agreement with the literature reported studies [42,43]. Comparative analysis of the average diameter of the primary particles of the soot samples was performed using the ImageJ software, wherein around 50 particles were analysed and the corresponding histogram distribution is presented in Fig. 5C, F.

The average particle diameter for diesel soot was recorded as 32 nm, while that of NBD10 soot was around 22 nm. This suggests that the addition of norbornane to diesel could lead to a greater degree of internal oxidation resulting in the reduction in the size of primary soot particles. Such small primary particles are known to have greater degree of surface carbon atoms which can be easily oxidised by air or NO_2 in DPF or via exhaust gas recirculation (EGR) to further reduce soot emission. The possibility of such reductions in soot emission can be further confirmed by analysing the internal fringe structure of soot particles by estimating the degree of fringe tortuosity and fringe length distribution in the primary soot particles.

A quantitative analysis of fringe length and tortuosity was performed using a Matlab code based on the algorithms reported in [44], wherein, the HRTEM image was subjected to negative transformation and grayscale. The negative transformation is defined as $I_{negetive} = L\text{-}1\text{-}I_{original}$, where L is the discrete intensity levels (256 per image), and $I_{original}$ is the image pixel value before transformation. On selected multiple regions of interest (ROI), operations like Gaussian filter, histogram equalization, and Tophat transformation were performed in order to eliminate errors due to non-homogeneous illumination across the image as well as to improve the fringe contrast. The branches from fringes were removed by a processes called skeletonization using built-in functions in Matlab that uses parallel thinning algorithm [45]. The lattice fringes in the image after skeletonization are reduced to 8-connected strokes or rings. With reference to these branch points, fringe length was determined in all directions. The smallest branch was identified, and the branch connections were broken by setting the first pixel to this branch as zero. The detailed procedure, equations, and algorithms used are already listed in detail in reference [44] and therefore shall not be repeated here. For each sample, an HRTEM image

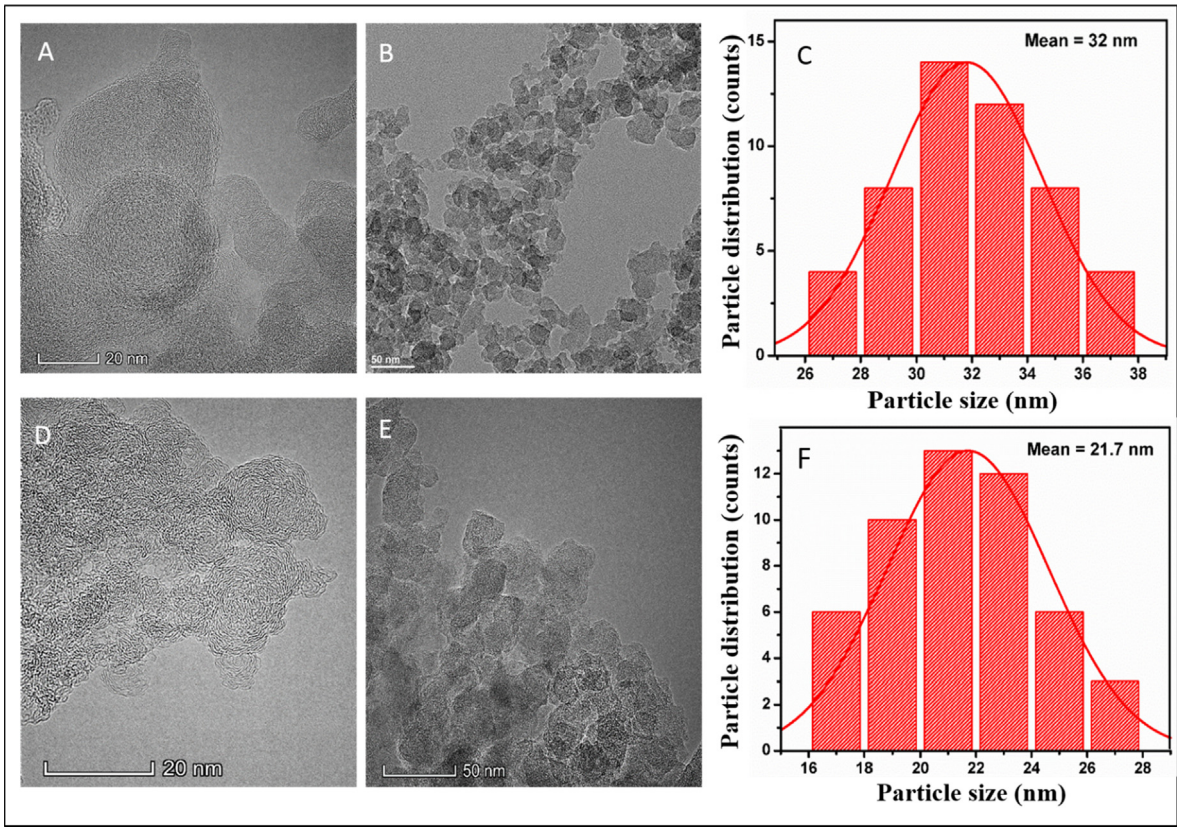

Fig. 5. HRTEM images and particle size distribution of Diesel soot (A, B, C) and NBD soot (D, E, F) at 20 nm and 50 nm resolutions, respectively.

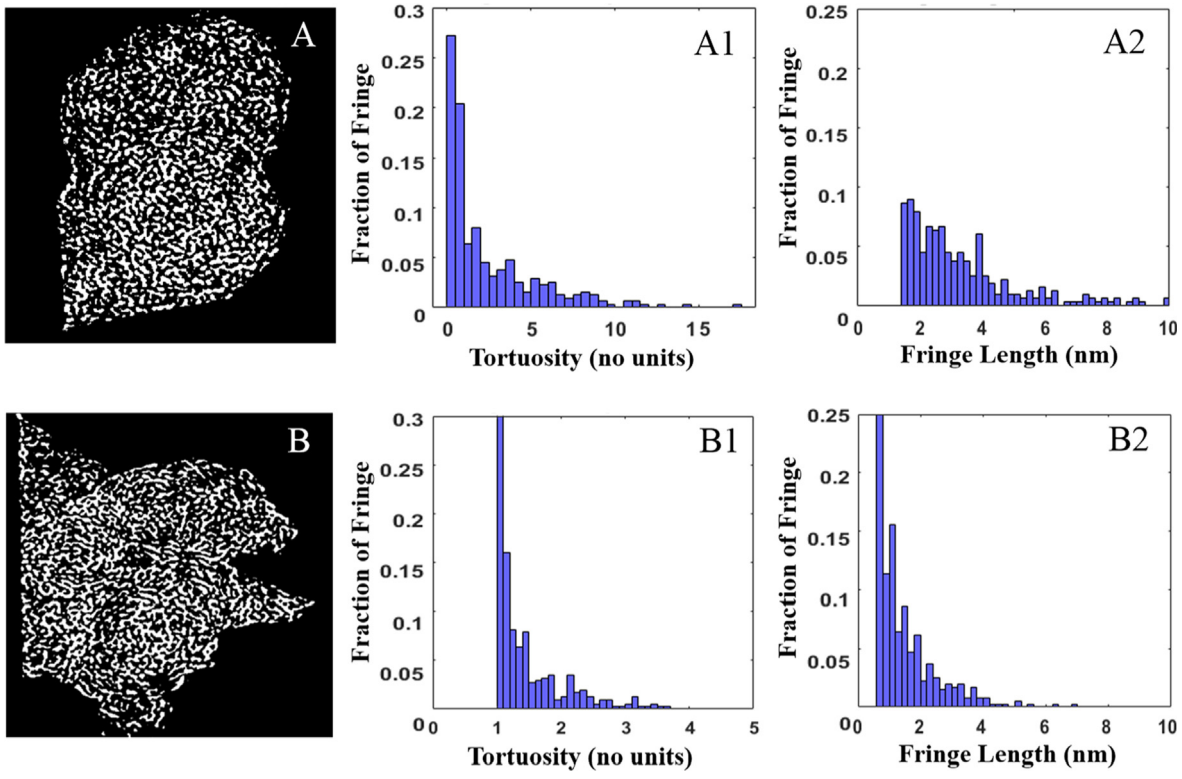

Fig. 6. Matlab processed images, fringe length and tortuosity index distribution of A) diesel soot and B) NBD10 soot.

consisting of 50–100 particles is chosen for homogeneity of primary particle structure, of which 5 high resolution microstructural images of each primary particle are randomly chosen, each consisting of > 100 fringe microstructures and is subjected to Matlab image processing as discussed above. The mean values of the fringe length and fringe tortuosity are then calculated using the Matlab code. The processed fringe structures and images for pure diesel and NBD soots are shown in Fig. 6. The quantitative data on the mean fringe length and Mean fringe curvature (i.e. tortuosity index) distribution is presented in Fig. 6, and the estimated values are listed in Table 2. From this table, one can conclude that diesel soot particles had a large mean fringe length of 3.57 nm which drastically decreases to 1.8 nm in the case of NBD10 soot. Moreover, the analysis of the tortuosity index also suggests that the short fringes in NBD10 soot have higher curvature (1.54) as compared to diesel soot (1.46). The tortuosity index measures the curvature of graphene layers (fringes), which usually develops from the formation of 5- and 7-membered ring structures within the planar aromatic framework of graphene layers. Such curvatures in aromatic layers prevent the development of long range graphitic stacks, resulting in the reduction in PAH stack size and overall primary particle size of the NBD10 soot [15]. Therefore, it is very clear that shorter fringe length and largely curved fringes together make the NBD10 soot highly disordered or amorphous, and hence, these soot samples are prone to easy oxidation as desired for the fast regeneration of DPF filters. The disorder in the crystal structure of these soot samples is further analysed using XRD and Raman spectroscopy.

3.5. X-ray diffraction

The X-ray diffraction analysis were performed on the NBD10 soot alongside the pure diesel soot, and the results are shown in Fig. 7. Two peaks at 2θ scale values of around 25° and 44° were observed. The peak at 2θ value of 25° is assigned to the (0 0 2) plane, and it contains the information about PAH interlayer spacing and thickness of the PAH stack. The peak at 2θ value of 44° is assigned to the (1 0 0) plane, and is an indicator of the average size of the PAH in the soot sample. The quantitative analysis of these two peaks provides information about the nanostructures of soot. These parameters manifest in the PAH interlayer spacing (d_{002}) as per Bragg's law (see equation E2), the nano-crystallite height (L_c), which gives the thickness of the PAH stack using Scherrer formula (see Equation E3), and the nano-crystallite width (L_a), which provides the average size of the PAH stack using Equation E4.

$$d_{002} = \frac{\lambda}{2sin\theta_{002}} \quad (2)$$

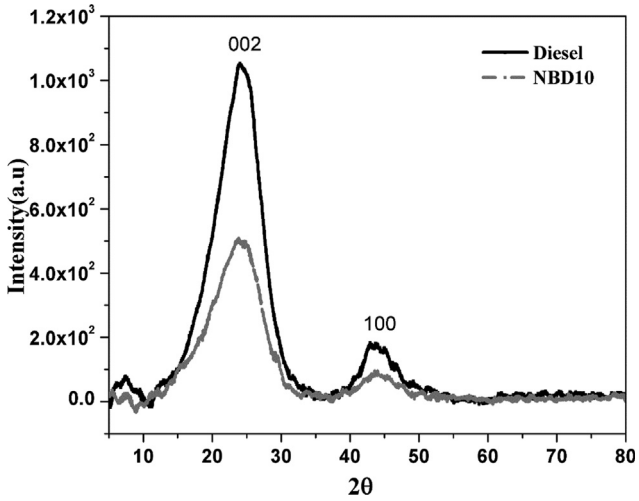

Fig. 7. XRD pattern of soot samples derived from Diesel and NBD10.

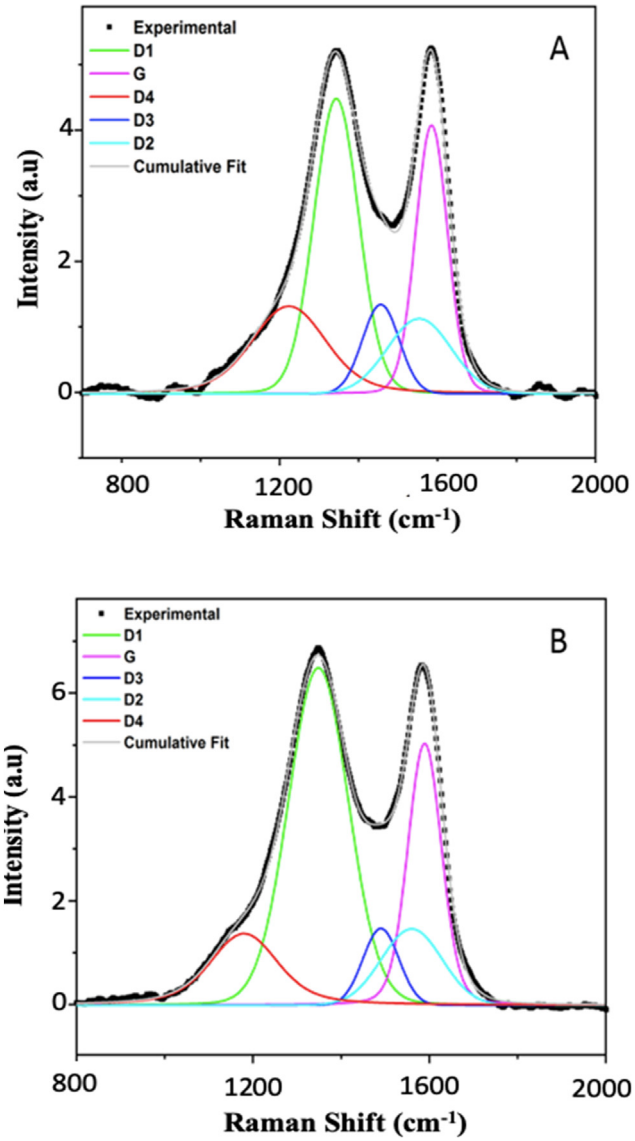

Fig. 8. Raman spectra for A) Diesel soot and B) NBD10 soot.

$$L_c = \frac{0.9\lambda}{B_{002}cos\theta_{002}} \quad (3)$$

$$L_a = \frac{1.84\lambda}{B_{100}cos\theta_{100}} \quad (4)$$

In these equations, λ = wavelength of X-ray (0.154 nm for Cu Kα), θ_{002} and θ_{001} are the Braggs angles, and B_{002} and B_{100} are the full width at half maximum (FWHM) for the two peaks. The Braggs angles and the FWHM were obtained via Gaussian fitting of the respective peaks using Matlab software. The obtained values are listed in Table 2.

As evident from Table 2, the interlayer separation between the PAH stacks is increased slightly in the case of NBD soot, which indicates a greater degree of disorder in the soot structure due to the addition of norbornane to diesel, although the difference is minimal. The L_a and L_c values confirm that the nano crystallites present in NBD10 soot sample contain smaller PAH stacks with reduced number of graphene layers per stack as compared to diesel soot, which is in agreement with the HRTEM analysis.

3.6. Raman spectroscopy

The Raman bands observed in the region of 900–2000 cm^{-1} for the

two soot samples are presented in Fig. 8. The first peak, observed at around 1350 cm^{-1}, is known as the D band, and it is associated with the disordered or aliphatic content of soot particles. The second peak at around 1590 cm^{-1} is known as the G band, and it is associated with the ordered or the graphitic structure of soot [46,47]. In order to analyse the Raman spectra, the 5-curve deconvolution model was used, wherein the raw experimental data were fitted using Voigt function, as suggested in [48]. The 5 fitted peaks were labelled as D1 = 1345 cm^{-1}, D2 = 1560 cm^{-1}, D3 = 1445 cm^{-1}, D4 = 1220 cm^{-1}, and G = 1590 cm^{-1}. The D2 and D3 bands represent the lattice vibrations and the existence of highly amorphous carbon in the soot samples, respectively. The intensity ratio of the D to G band is used as an indicator of the magnitude of discontinuity and randomness of graphene layers present in soot [48,49]. The ratio of D band intensity over the G band intensity (I_D/I_G) is related to the lattice width (L_a) through Knight and White equation (E5) [50]. The intensity of the D1 peak is used here instead of D along with a proportionality constant of 4.4 for the excitation wavelength of 515 nm, as suggested in references [50,51]. The calculated values of L_a and I_{D1}/I_G are listed in Table 2.

$$L_a = 4.4\left(\frac{I_{D1}}{I_G}\right)^{-1} \quad (5)$$

As evident from the obtained values, the I_{D1}/I_G ratio of NBD10 soot is higher than that of diesel soot. The calculated values of L_a using Raman data have the same trend as those obtained from XRD studies, although the L_a values calculated using the former method are relatively higher. The higher intensity of I_{D1} peak is a clear indicator of greater disorder in the soot structure leading to smaller PAH stacks in NBD10 soot as compared to diesel soot. Therefore, both the XRD and the Raman studies very well complement each other and are in excellent agreement with the HRTEM results presented earlier, which concluded the existence of shorter graphene fringes with increased tortuosity that lead to greater disorder in NBD10 soot. The smaller size of the PAH stack with increased disorder results in the increased exposure of edge carbon atoms to the reactive species such as radicals and O_2 to augment the oxidation kinetics of NBD10 soot. The greater degree of curvature also reduces the stability of the PAH stack, thus reducing the activation energy for the oxidation of soot particles, as observed in the TGA studies.

3.7. Elemental analysis (EDX)

Several studies in the literature have indicated that the percentage of oxygen functionalities in the additive, especially biofuels, induces greater oxygen content in the soot samples, which ultimately increases soot oxidation rate [49] and lowers the activation energy of its oxidation. Since norbornane does not contain any oxygenated functional group in its chemical structure, such a contribution to oxygen content of the soot may not be expected. However, to verify this hypothesis, it was important to measure the relative C/O ratio on the blended samples. In order to qualitatively approximate the distribution of carbon and oxygen atoms on the surface of soot samples, the samples were coated with Au/Pd by sputtering method on an aluminium foil and the Energy Dispersive X-ray Spectra (EDX) are recorded using Ametex EDX PV6500 system. The data was processed using eZAF Smart Quant analyser. The results of this analysis on both the soots are shown in Fig. 9. The atomic and weight percentages of carbon and oxygen atoms in three different regions (A1-A3) of each soot sample were measured [42]. It is evident from Fig. 9 that NBD10 soot contains approximately 6 (± 1)% more oxygen content than the diesel soot. The C/O ratio in NBD10 soot is 1.54, while that in diesel soot is 1.94. The greater percentage of oxygen content in NBD10 soot in spite of the lack of oxygen functionalities in norbornane structure suggests that there is no direct correlation between the additive oxygen functionalities and soot oxygen content. The higher oxygen content in NBD10 soot is, therefore, a result its greater oxidation in flames due to increased crystal disorder. Its higher oxygen content also supports its higher oxidative reactivity, as observed in TGA analysis.

3.8. Electron energy loss spectroscopy (EELS)

Electron Energy Loss Spectroscopy (EELS) is very effective for the quantitative analysis of the relative distribution of sp^3 and sp^2 hybridized carbons in soot samples. The qualitative estimation of the peak positions and the intensity ratio of *1 s* to π* and *1 s* to σ* K edge transitions are noted [52]. The aliphatic/aromatic distribution of the soot samples is further analyzed using the ratio of the two peak intensities, denoted by π*/σ*. A high π*/σ* ratio is an indicator of a greater amount of aromatic hydrocarbons (π bonding) and a low amount of aliphatic functionalities in the sample. When the EELS spectrum of the diesel and the NBD10 soot samples are compared (see Fig. 10), significant differences in the π* (287 eV) and σ* (295 eV) are observed. The σ* peak with broad hump like structure in case of soot collected from NBD confirms that these soots have highly disorder graphene layers [53] (in agreement with the HRTEM, XRD, and Raman studies).

The obtained π*/σ* ratios were 0.775 for pure diesel and 0.632 for the NBD10, which indicates that the NBD10 soot has a higher aliphatic content as compared to the pure diesel soot. Aliphatic compounds are known to undergo rapid oxidation as compared to aromatics. At lower oxidation temperatures, easy oxidation of the aliphatic chains results in the reduction in the size of soot particles with a greater amount of aromatic content still intact. As higher conversion levels are reached, the elimination of smaller PAH and aliphatic chains leaves the soot with long range PAHs, which require higher activation energy to be overcome for oxidation, as observed during TGA analysis of NBD10 soot. Due to the existence of a greater extent of graphitic character in diesel soot, the increase in activation energy for soot oxidation at higher conversion levels was insignificant in this case. Therefore, EELS studies compliment the observations made on the reactivity of soot samples in the TGA [52].

3.9. Structural comparison between NBD10 and Dicyclopentadiene-diesel soot nanostructures

All the above investigations confirmed that the introduction of a saturated 5-membered bicyclic additive, norbornane significantly alters the soot nanostructure of diesel and induces greater fringe curvature/disorders in the soot structure with increased oxidative reactivity. Such improved oxidative reactivity supresses soot emission rate during diesel combustion. Since norbornane is a saturated bicyclic additive, it is interesting to qualitatively compare its effect on soot nanostructural parameters with another 5-membered bicyclic but unsaturated additive, DCPD, studied in [22]. Such a comparison is interesting from industrial point of view because DCPD serves as a precursor for the manufacturing of norbornane. Moreover, both are also found in crude oil distillates in refineries. Such a comparison could provide some important information, useful for deciding distillation methodologies. In order to compare the two soots, the normalized nanostructural parameters, PAH stack width (NL_a), mean primary particle size (NS), aromatic/aliphatic content ($N\pi^*/\sigma^*$) ratio, and activation energy (NEa) for soot oxidation for NBD10 and DCPD10 soots [22] were compared (the parameter values were normalized with the values for pure diesel soot in the two studies), and the values are shown in Table 3.

The normalised NL_a and NS values of NBD10 were found to be 0.87 and 0.67, while those of DCPD10 soot were 0.93 and 0.75, respectively. The consistently lower values suggest that norbornane addition to diesel has a greater tendency to reduce the PAH stack size and mean particle size, which is beneficial, as increases the effective surface area and exposes a greater number of reactive edge carbon atoms to the incoming oxygen or radical species to induce a faster rate of oxidation

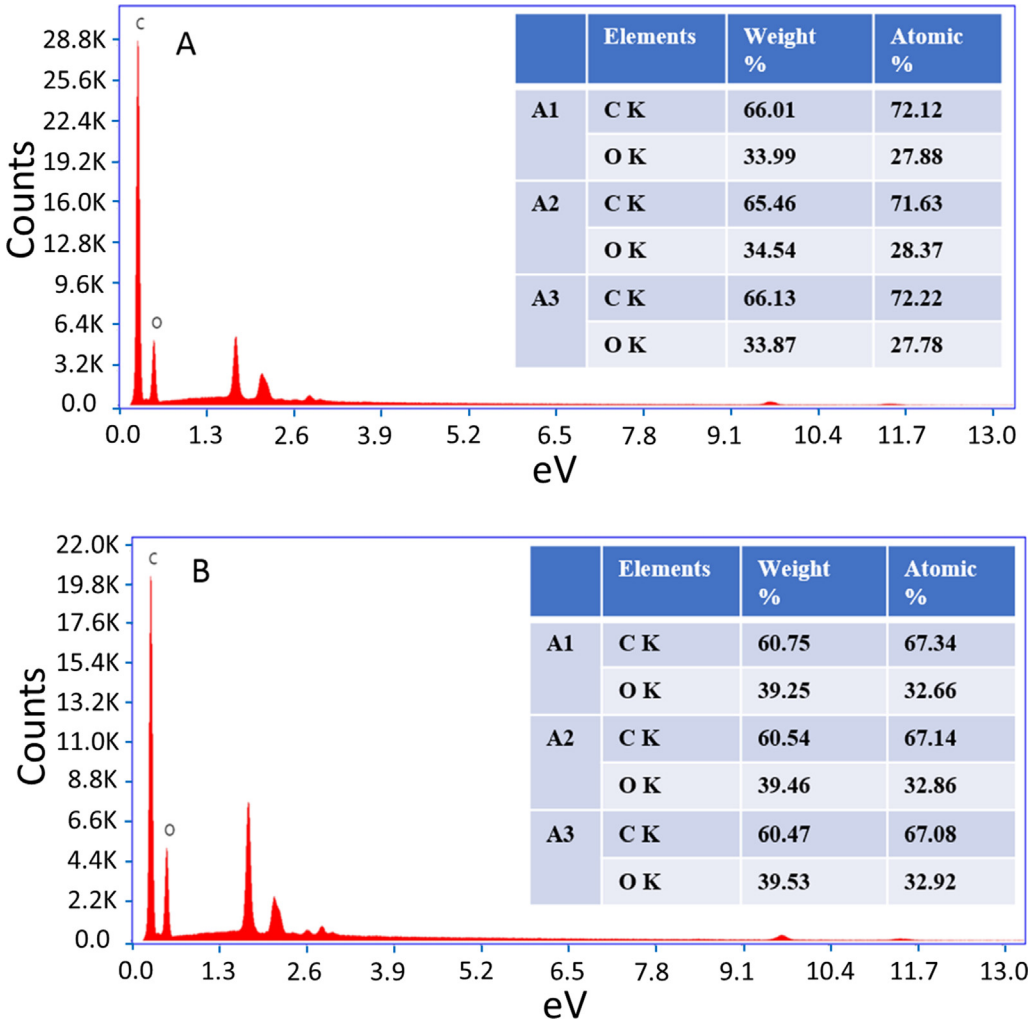

	Elements	Weight %	Atomic %
A1	C K	66.01	72.12
	O K	33.99	27.88
A2	C K	65.46	71.63
	O K	34.54	28.37
A3	C K	66.13	72.22
	O K	33.87	27.78

	Elements	Weight %	Atomic %
A1	C K	60.75	67.34
	O K	39.25	32.66
A2	C K	60.54	67.14
	O K	39.46	32.86
A3	C K	60.47	67.08
	O K	39.53	32.92

Fig. 9. Elemental composition of A) diesel soot and B) NBD10 soot.

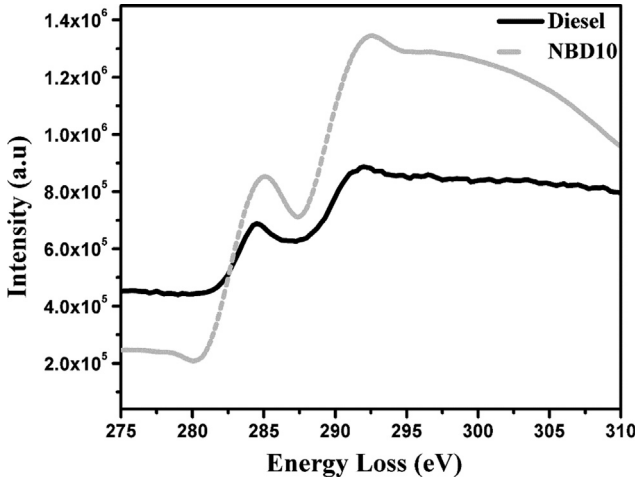

Fig. 10. EELS spectra for diesel soot and NBD10 soot.

and improves soot suppression efficiency. A comparison of the normalized ratio of π^*/σ^* suggests that DCPD10 soot ($N\pi^*/\sigma^* = 0.92$) had an overall greater aromatic content and lower aliphatic content as compared to NBD10 soot ($N\pi^*/\sigma^* = 0.82$). The normalised activation energy for soot oxidation measured in TGA supports this observation, as the obtained normalised NE_a of 0.65 is significantly lower in case of NBD10 soot, as compared to DCPD10 soot having NE_a of 0.88. Such a difference in the soot nanostructure, degree of disorder, and aromatic/aliphatic composition resulting in significantly different oxidative reactivity could arise due to the differences in the thermal decomposition behaviour of NBD and DCPD during the early ignition phase of the fuel blend. This could result in the variation in the type of primary radical species generated, their relative stabilization effects, radical propagation, and branching reactions during the combustion of fuel blend, all of which directly affect the rate of diesel fuel oxidation and soot formation mechanisms. The combustion product analysis studies for such bicyclic fuels, therefore, could be interesting for future research. This study therefore concludes that the saturated 5-membered bicyclic additives such as norbornane serves as an efficient additive and has excellent soot suppression potential. More importantly, this study also confirms that the 5-membered bicyclic compounds such as norbornane and dicyclopentadiene, which are available as by-products of existing chemical processing industries, are promising alternative fuel additives to diesel, and could be retained during oil distillation process to form an integral

Table 3
Normalized NBD10 and DCPD10 soot nanostructural parameters calculated with respect to diesel soot.

Soot sample	NL_a	NS	$N\pi^*/\sigma^*$	NE_a
NBD10	0.87	0.67	0.82	0.65
DCPD10	0.93	0.75	0.92	0.88
Diesel soot	1	1	1	1

component of fuel formulation.

4. Conclusion

A systematic investigation on the addition of norbornane, a saturated, 5 membered-bicyclic additive to diesel on its fuel properties, soot nanostructure and oxidative reactivity was performed. The sooting propensity of diesel was found to decrease at an optimum blending percentage of 10% norbornane-90% diesel. The decrease in sooting propensity of the blend was found to be a result of the enhanced internal oxidation of soot particles, as they travel through the flame. Thermogravimetric analysis revealed that the NBD10 soot had a significantly lower initial activation energy for oxidation as compared to pure diesel soot. Detailed morphological characterization of the soot samples using HRTEM, XRD, Raman, EDX and EELS techniques revealed that, the greater oxidative reactivity of NBD10 soot is a result of increased structural disorder (greater fringe tortuosity, shorter fringe length), smaller primary particle size, and the greater percentages of oxygen and aliphatic functionalities in the soot structure. A qualitative comparison between nanostructural characteristics and oxidative reactivity of soots obtained from 5-membered bicyclic additives, norbornane (saturated compound) and dicyclopentadiene (unsaturated compound) suggests that the saturated bicyclic additives have a relatively greater soot suppression potential. More importantly, this investigation confirms that 5-membered bicyclic additives, which are readily available as by-products of chemical industries can serve as potential fuel additives and therefore should be utilized in designing advanced fuel formulations.

CRediT authorship contribution statement

Moataz K. Abdrabou: Data curation, Formal analysis, Investigation, Visualization, Writing - original draft. **Pranay P. Morajkar:** Data curation, Formal analysis, Investigation, Visualization, Writing - review & editing. **Gerardo D.J. Guerrero Peña:** Data curation, Formal analysis, Investigation, Visualization. **Abhijeet Raj:** Conceptualization, Funding acquisition, Project administration, Resources, Supervision, Writing - review & editing. **Mirella Elkadi:** Funding acquisition, Project administration, Resources. **Akshay V. Salkar:** Data curation.

Declaration of Competing Interest

The authors declare that they have no known competing financial interests or personal relationships that could have appeared to influence the work reported in this paper.

Acknowledgement

The authors would like to acknowledge the financial support received from Khalifa University of Science & Technology (CIRA-2018-99) U.A.E and instrumental facilities support of Goa University, India (via DST/IMRCD/INNO-INDIGO/BioCFD/2017(G)) in order to accomplish this work. This publication is based upon work supported by the Khalifa University of Science and Technology under Award No. RC2-2018-024.

References

[1] Stanmore BR, Brilhac JF, Gilot P. The oxidation of soot: A review of experiments, mechanisms and models. Carbon N. Y. 2001;39(15):2247–68.
[2] Silverman DT, Samanic CM, Lubin JH, Blair AE, Stewart PA, Vermeulen R, et al. The diesel exhaust in miners study: A nested case-control study of lung cancer and diesel exhaust. J. Natl. Cancer Inst. 2012;104(11):855–68.
[3] Heeb NV, Schmid P, Kohler M, Gujer E, Zennegg M, Wenger D, et al. Secondary effects of catalytic diesel particulate filters: Conversion of PAHs versus formation of Nitro-PAHs. Environ. Sci. Technol. 2008;42(10):3773–9.
[4] Brijesh P, Sreedhara S. Exhaust emissions and its control methods in compression ignition engines: A review. Int. J. Automot. Technol. 2013;14(2):195–206.
[5] Beatrice C, Costagliola MA, Guido C, Napolitano P, Prati MV. How Much Regeneration Events Influence Particle Emissions of DPF-Equipped Vehicles? SAE Tech. Pap. 2017;vol. 2017-Septe:4271.
[6] Dias V, Katshiatshia HM, Jeanmart H. The influence of ethanol addition on a rich premixed benzene flame at low pressure. Combust. Flame 2014;161(9):2297–304.
[7] Morajkar P, Schoemaecker C, Okumura M, Fittschen C. Direct measurement of the equilibrium constants of the reaction of formaldehyde and acetaldehyde with HO2 radicals. Int. J. Chem. Kinet. 2014;46(5):245–59.
[8] Morajkar P, Bossolasco A, Schoemaecker C, Fittschen C. Photolysis of CH3CHO at 248 nm: Evidence of triple fragmentation from primary quantum yield of CH3and HCO radicals and H atoms. J. Chem. Phys. 2014;140(21).
[9] Morajkar P, Schoemaecker C, Fittschen C. Absolute absorption cross sections for two selected lines of formaldehyde around 6625 cm-1. J. Mol. Spectrosc. 2012;281(1):18–23.
[10] He C, Li J, Wang Y, Tan J, Song G, Jia D, et al. Size-segregated particulate matter emission characteristics of a heavy-duty diesel engine with oxygenated fuels. Appl. Therm. Eng. 2017;125:1173–80.
[11] Knothe G, Steidley KR. Lubricity of Components of Biodiesel and Petrodiesel. The Origin of Biodiesel Lubricity. Energy Fuels May 2005;19(3):1192–200.
[12] Niculescu R, Clenci A, Iorga-Siman V. Review on the use of diesel-biodiesel-alcohol blends in compression ignition engines. Energies 2019;12(7):1–41.
[13] Manoj B, Kunjomana AG. Study of stacking structure of amorphous carbon by X-ray diffraction technique. Int. J. Electrochem. Sci. 2012;7(4):3127–34.
[14] Botero ML, Adkins EM, González-Calera S, Miller H, Kraft M. PAH structure analysis of soot in a non-premixed flame using high-resolution transmission electron microscopy and optical band gap analysis. Combust. Flame 2016;164:250–8.
[15] Yehliu K, Vander Wal RL, Armas O, Boehman AL. Impact of fuel formulation on the nanostructure and reactivity of diesel soot. Combust. Flame, Dec. 2012;159(12):3597–606.
[16] Raj A, da Silva GR, Chung SH. Reaction mechanism for the free-edge oxidation of soot by O2. Combust. Flame 2012;159(11):3423–36.
[17] Lapuerta M, Rodríguez-Fernández J, Sánchez-Valdepeñas J. Soot reactivity analysis and implications on diesel filter regeneration. Prog. Energy Combust. Sci. 2020;78.
[18] Martin JW, Bowal K, Menon A, Slavchov RI, Akroyd J, Mosbach S, et al. Polar curved polycyclic aromatic hydrocarbons in soot formation. Proc. Combust. Inst. 2019;37(1):1117–23.
[19] X. Z. Wu, R. Yang M. M. Chen, H. R. Tian, J. Xiao, Y.Y. Xu, M. S. Lin, L. Abella,, C. B. Tian, C. L. Gao, Q. Zhang, S. Y. Xie, R. B. Huang, L. S. Zheng,, "Formation of Curvature Subunit of Carbon in Combustion," J. Am. Chem. Soc., vol. 138, no. 30, pp. 9629–9633, 2016.
[20] Vander Wal RL, Tomasek AJ. Soot oxidation: Dependence upon initial nanostructure. Combust. Flame 2003;134(1–2):1–9.
[21] R. E. Kroto, H. W.; Heath, J. R.; Obrien, S. C.; Curl, R. F.; Smalley, "C60: Buckminsterfullerene," Nature, vol. 318, no. 6042, pp. 162–163, 1985.
[22] Alrefaai MM, Guerrero Peña GDJ, Raj A, Stephen S, Anjana T, Dindi A. Impact of dicyclopentadiene addition to diesel on cetane number, sooting propensity, and soot characteristics. Fuel 2017, 2018,;216(December):110–20.
[23] Guerrero Peña GDJ, Alrefaai MM, Yang SY, Raj A, Brito JL, Stephen S, Anjana T, Pillai V, Al Shoaibi A, Chung SH. Effects of methyl group on aromatic hydrocarbons on the nanostructures and oxidative reactivity of combustion-generated soot. Combust. Flame 2016;172:1–12.
[24] Glassman I. Soot formation in combustion processes. Symp. Combust. 1989;22(1):295–311.
[25] Yang Y, Boehman AL, Santoro RJ. A study of jet fuel sooting tendency using the threshold sooting index (TSI) model. Combust. Flame 2007;149(1–2):191–205.
[26] Neer A, Koylu UO. Effect of operating conditions on the size, morphology, and concentration of submicrometer particulates emitted from a diesel engine. Combust. Flame 2006;146(1):142–54.
[27] Armas O, Hernández JJ, Cárdenas MD. Reduction of diesel smoke opacity from vegetable oil methyl esters during transient operation. Fuel 2006;85(17):2427–38.
[28] Zannis TC, Hountalas DT, Papagiannakis RG, Levendis YA. Effect of Fuel Chemical Structure and Properties on Diesel Engine Performance and Pollutant Emissions. SAE Int. J. Fuels Lubr. Mar. 2009;1(1):384–419.
[29] Watson RJ, Botero ML, Ness CJ, Morgan NM, Kraft M. An improved methodology for determining threshold sooting indices from smoke point lamps. Fuel 2013;111:120–30.
[30] Peña GDJG, Rahman RK, Raj A, Stephen S, Anjana T, Brito JL. Effect of fuel flow rate on the characteristics of soot generated from unsubstituted and disubstituted aromatic hydrocarbon flames: Experimental and numerical study. Combust. Flame 2018;190:224–39.
[31] ASTM D975-20, Standard Specification for Diesel Fuel, ASTM International, West Conshohocken, PA, 2020, www.astm.org.
[32] Ejim CE, Fleck BA, Amirfazli A. Analytical study for atomization of biodiesels and their blends in a typical injector: Surface tension and viscosity effects. Fuel 2007;86(10–11):1534–44.
[33] Calcote HF, Manos DM. Effect of molecular structure on incipient soot formation. Combust. Flame 1983;49(1–3):289–304.
[34] Meng Z, Yang D, Yan Y. Study of carbon black oxidation behavior under different heating rates. J. Therm. Anal. Calorim. 2014;118(1):551–9.
[35] Friedman HL. Kinetics of thermal degradation of char-forming plastics from thermogravimetry. Application to a phenolic plastic. J. Polym. Sci. Part C Polym. Symp. 1964;6(1):183–95.
[36] Elder JP. Reconciliation of Arrhenius and iso-conversional analysis kinetics parameters of non-isothermal data. Thermochim. Acta 1996;272(1–2):41–8.

[37] Vyazovkin S, Burnham AK, Criado JM, Pérez-Maqueda LA, Popescu C, Sbirrazzuoli N. ICTAC Kinetics Committee recommendations for performing kinetic computations on thermal analysis data. Thermochim. Acta 2011;520(1–2):1–19.
[38] Sharma HN, Pahalagedara L, Joshi A, Suib SL, Mhadeshwar AB. Experimental study of carbon black and diesel engine soot oxidation kinetics using thermogravimetric analysis. Energy and Fuels 2012;26(9):5613–25.
[39] Raj A, Tayouo R, Cha D, Li L, Ismail MA, Chung SH. Thermal fragmentation and deactivation of combustion-generated soot particles. Combust. Flame 2014;161(9):2446–57.
[40] Raj A, da Silva GR, Chung SH. Reaction mechanism for the free-edge oxidation of soot by O2. Combust. Flame Nov. 2012;159(11):3423–36.
[41] Chaparala SV, Raj A. Reaction mechanism for the oxidation of zigzag site on polycyclic aromatic hydrocarbons in soot by O2. Combust. Flame Mar. 2016;165:21–33.
[42] D. Zhang, Y. Ma, and M. Zhu, "Nanostructure and oxidative properties of soot from a compression ignition engine : The effect of a homogeneous combustion catalyst," vol. 34, pp. 1869–1876, 2013.
[43] Szybist JP, Song J, Alam M, Boehman AL. Biodiesel combustion, emissions and emission control. Fuel Process. Technol. Jul. 2007;88(7):679–91.
[44] Yehliu K, Vander Wal RL, Boehman AL. Development of an HRTEM image analysis method to quantify carbon nanostructure. Combust. Flame 2011;158(9):1837–51.
[45] Lam L, Lee S-, Suen CY. Thinning methodologies-a comprehensive survey. IEEE Trans. Pattern Anal. Mach. Intell. 1992;14(9):869–85.
[46] Sadezky A, Muckenhuber H, Grothe H, Niessner R, Pöschl U. Raman microspectroscopy of soot and related carbonaceous materials: Spectral analysis and structural information. Carbon N. Y. Jul. 2005;43(8):1731–42.
[47] Salamanca M, Mondragón F, Agudelo JR, Benjumea P, Santamaría A. Variations in the chemical composition and morphology of soot induced by the unsaturation degree of biodiesel and a biodiesel blend. Combust. Flame Mar. 2012;159(3):1100–8.
[48] Catelani T, Pratesi G, Zoppi M. Raman characterization of ambient airborne soot and associated mineral phases. Aerosol Sci. Technol. 2014;48(1):13–21.
[49] Morajkar, P. P. G. D.J. Guerrero Penã, A. Raj, M. Elkadi, R. K. Rahman, A. V. Salkar, A. Pillay, A. Tharalekshmy, M. S. Cha, "Effects of Camphor Oil Addition to Diesel on the Nanostructures and Oxidative Reactivity of Combustion-Generated Soot," Energy and Fuels, vol. 33, no. 12, pp. 12852–12864, 2019.
[50] Escribano R, Sloan JJ, Siddique N, Sze N, Dudev T. Raman spectroscopy of carbon-containing particles. Vib. Spectrosc. 2001;26(2):179–86.
[51] G. D. J. Guerrero Peña, Y. A. Hammid, A. Raj, S. Stephen, T. Anjana, and V. Balasubramanian, "On the characteristics and reactivity of soot particles from ethanol-gasoline and 2,5-dimethylfuran-gasoline blends," Fuel, vol. 222, no. February, pp. 42–55, 2018.
[52] Al-Qurashi K, Boehman AL. Impact of exhaust gas recirculation (EGR) on the oxidative reactivity of diesel engine soot. Combust. Flame 2008;155(4):675–95.
[53] Braun A, Huggins FE, Shah N, Chen Y, Wirick S, Mun SB, Jacobsen C, Huffman GP. Advantages of soft X-ray absorption over TEM-EELS for solid carbon studies—a comparative study on diesel soot with EELS and NEXAFS. Carbon N. Y. 2005;43(1):117–24.